2015

Morphological Transformations in the Magnetite Biomineralizing Protein Mms6 in Iron Solutions: A Small-Angle X-ray Scattering Study

Honghu Zhang
Iowa State University, hhzhang@iastate.edu

Xunpei Liu
Iowa State University, xpliu@iastate.edu

Shuren Feng
Iowa State University, sfeng@iastate.edu

Wenjie Wang
Iowa State University, wwang@ameslab.gov

Klaus Schmidt-Rohr
Iowa State University, srohr@iastate.edu

See next page for additional authors

Morphological Transformations in the Magnetite Biomineralizing Protein Mms6 in Iron Solutions: A Small-Angle X-ray Scattering Study

Abstract

Magnetotactic bacteria that produce magnetic nanocrystals of uniform size and well-defined morphologies have inspired the use of biomineralization protein Mms6 to promote formation of uniform magnetic nanocrystals *in vitro*. Small angle X-ray scattering (SAXS) studies in physiological solutions reveal that Mms6 forms compact globular three-dimensional (3D) micelles (approximately 10 nm in diameter) that are, to a large extent, independent of concentration. In the presence of iron ions in the solutions, the general micellar morphology is preserved, however, with associations among micelles that are induced by iron ions. Compared with Mms6, the m2Mms6 mutant (with the sequence of hydroxyl/carboxyl containing residues in the C-terminal domain shuffled) exhibits subtle morphological changes in the presence of iron ions in solutions. The analysis of the SAXS data is consistent with a hierarchical core–corona micellar structure similar to that found in amphiphilic polymers. The addition of ferric and ferrous iron ions to the protein solution induces morphological changes in the micellar structure by transforming the 3D micelles into objects of reduced dimensionality of 2, with fractal-like characteristics (including Gaussian-chain-like) or, alternatively, platelet-like structures.

Disciplines

Biochemistry, Biophysics, and Structural Biology | Biological and Chemical Physics | Materials Chemistry | Organic Chemistry | Other Chemistry

Comments

Reprinted (adapted) with permission from Langmuir, 2015, 31 (9), pp 2818–2825, **DOI:** 10.1021/la5044377.

Authors

Honghu Zhang, Xunpei Liu, Shuren Feng, Wenjie Wang, Klaus Schmidt-Rohr, Mufit Akinc, Marit Nilsen-Hamilton, David Vaknin, and Surya K. Mallapragada

Langmuir

Article

pubs.acs.org/Langmuir

Morphological Transformations in the Magnetite Biomineralizing Protein Mms6 in Iron Solutions: A Small-Angle X-ray Scattering Study

Honghu Zhang,[†,‡] Xunpei Liu,[†,¶] Shuren Feng,[†,§] Wenjie Wang,*[,†] Klaus Schmidt-Rohr,[†,∥] Mufit Akinc,[†,‡] Marit Nilsen-Hamilton,[†,§] David Vaknin,[†,⊥] and Surya Mallapragada*[,†,¶]

[†]Division of Materials Science and Engineering, Ames Laboratory, USDOE, Ames, Iowa 50011, United States

[‡]Department of Materials Science and Engineering, [¶]Department of Chemical and Biological Engineering, [§]Roy J. Carver Department of Biochemistry, Biophysics and Molecular Biology, [∥]Department of Chemistry, and [⊥]Department of Physics and Astronomy, Iowa State University, Ames, Iowa 50011, United States

ABSTRACT: Magnetotactic bacteria that produce magnetic nanocrystals of uniform size and well-defined morphologies have inspired the use of biomineralization protein Mms6 to promote formation of uniform magnetic nanocrystals *in vitro*. Small angle X-ray scattering (SAXS) studies in physiological solutions reveal that Mms6 forms compact globular three-dimensional (3D) micelles (approximately 10 nm in diameter) that are, to a large extent, independent of concentration. In the presence of iron ions in the solutions, the general micellar morphology is preserved, however, with associations among micelles that are induced by iron ions. Compared with Mms6, the m2Mms6 mutant (with the sequence of hydroxyl/carboxyl containing residues in the C-terminal domain shuffled) exhibits subtle morphological changes in the presence of iron ions in solutions. The analysis of the SAXS data is consistent with a hierarchical core−corona micellar structure similar to that found in amphiphilic polymers. The addition of ferric and ferrous iron ions to the protein solution induces morphological changes in the micellar structure by transforming the 3D micelles into objects of reduced dimensionality of 2, with fractal-like characteristics (including Gaussian-chain-like) or, alternatively, platelet-like structures.

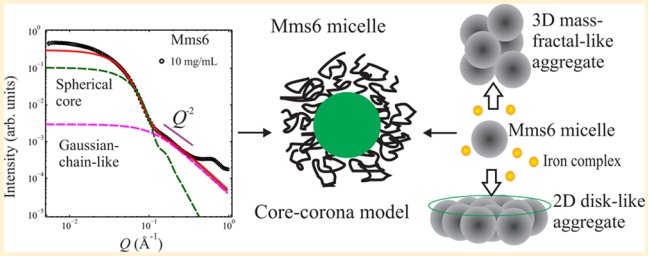

INTRODUCTION

It is well-known that many living organisms, whether unicellular or multicellular, are capable of developing complex inorganic−organic hierarchical materials for various functions such as skeletal support, protection, locomotion, and navigation.[1,2] These materials are intricately designed under physiological conditions through biomineralization with a high level of control on their particle sizes, morphologies, structures, compositions, aggregation, and crystallographic orientation, and hence exhibit remarkably controlled mechanical, optical, and magnetic properties.[1−3] Tremendous efforts have been devoted to investigating mechanisms of such biomineralization as well as gaining inspiration from nature to develop biomimetic synthetic routes for advanced functionalized materials.[4−7] Proteins and other biological macromolecules, interacting with mineral crystals in biological systems, play an important role in the controlled process of mineralization, which have attracted considerable research interest in recent decades.[8−10] For instance, magnetotactic bacteria, a diverse family of aquatic prokaryotes, have the particular ability to align with the geomagnetic field due to the presence of the magnetosome, an organelle made of a lipid vesicle, in which biomineralized magnetite (Fe_3O_4) or greigite (Fe_3S_4) crystals of uniform sizes and well-defined shapes are embedded.[11] Therefore, they have been employed as effective tools to study biomineralization of magnetic crystals.[12−14]

Mms6, one of several proteins tightly bound to the magnetosome magnetite crystal in magnetotactic bacteria *Magnetospirillum magneticum* AMB-1, has been implicated in the biomineralization of magnetite.[15−19] It has been shown to promote the formation of uniform superparamagnetic magnetite nanocrystals at room temperature and mild conditions *in vitro*.[15,20,21] In addition, Mms6 promotes *in vitro* synthesis of other advanced functionalized materials, such as cobalt ferrite, cobalt doped magnetite, and magnetic nanoparticle arrays.[22−26] Such magnetic materials synthesized with Mms6 have many promising potential applications in targeted drug delivery, magnetic resonance imaging (MRI) contrast agents, and high density data storage.[18] Therefore, significant research efforts have led to understanding the mechanism of Mms6 biomineralization *in vivo*,[16] synthesizing a variety of magnetic nanomaterials *in vitro*, and thereby expanding the biomineralization processes beyond natural materials.[22,25,26] Progress has been made recently in understanding the structure and properties of Mms6.[21,27] Mms6 is an amphiphilic protein with hydrophobic N-terminal and hydrophilic C-terminal, is believed to exist as a membrane protein *in vivo*, and self-assembles *in vitro* to form a multimeric micellar complex larger

Received: November 11, 2014
Revised: January 29, 2015
Published: February 10, 2015

DOI: 10.1021/la5044377
Langmuir 2015, 31, 2818−2825

than 300 kDa.[19,21,27,28] The C-terminal domains bind ferric iron ions and complexes with very high affinity.[21,28] Shuffling the amino acid sequence in a protein affects its function and thus is a good test to understand the mechanism of biomineralization. A C-terminal mutant, m2Mms6, has been designed that shows much lower iron binding than the wild-type Mms6.[21] Here, we further examine the global morphology of the protein and its C-terminal modified mutant to understand its role in biomineralization. The role of Mms6 in magnetite synthesis *in vitro* is still under investigation.[18−20] With the highly hydrophobic N-terminal domain and larger complex formed by Mms6, it is challenging to determine in detail how Mms6 interacts with iron precursors at atomic resolution by either X-ray crystallography or nuclear magnetic resonance (NMR) spectroscopy. Great caution has to be taken when interpreting data collected with "dry" methods such as AFM and TEM for biomacromolecules like Mms6 due to sample damage or distortion.[27] Here we report on synchrotron radiation small-angle X-ray scattering (SAXS) of Mms6 to determine its morphological characteristics in various solution conditions, as SAXS can provide an overall three-dimensional structural/morphological information for biological macromolecular complexes in solutions.[29,30]

Magnetite nanoparticles synthesized via the classical coprecipitation method by elevating the pH of a stoichiometric mixture of ferrous and ferric salts in aqueous medium at room temperature are mostly less than 20 nm and nonuniform in size.[31] In contrast, in the presence of Mms6, magnetite slowly grows to ∼30-nm-diameter superparamagnetic nanoparticles of uniform size and cuboctahedral shapes.[20,21] The interactions between Mms6 and iron are believed to be the initial steps of biomineralization, and also to be important in determining the shape of the magnetite nanoparticles.[16,21] The Mms6−iron interactions at various pH values have been previously investigated on aqueous surfaces, where Mms6 was deposited on the surface of an iron solute subphase to form a monolayer, taking advantage of its amphiphilic behavior.[28] In this SAXS study, we investigate the interactions of Mms6 with iron salts in Tris/KCl solutions under very similar conditions to room temperature *in vitro* synthesis of magnetite.[20,21] The role of pH in the morphology of the protein is also reported as a control in that the presence of iron in solutions affects the pH. The work presented here deals with the interaction of the biomineralization protein with the iron ions, which is the first step in the formation of magnetic nanoparticles using this bioinspired approach. However, the uniform nanoparticles are formed only after these Mms6/iron solutions are exposed to sodium hydroxide (see ref 20 for more details) to elevate the pH significantly and cause coprecipitation, and after a long incubation period of days, which is a step that we have not included in these SAXS studies, since we are studying the role of iron on Mms6. Therefore, in this study it is not intended to form magnetic nanoparticles. It is worth noting that the concentrations of proteins subjected to SAXS measurements are increased to the level of ∼1 mg/mL in order to achieve acceptable data quality, while most reported Mms6 concentrations used for magnetic nanocrystal synthesis are less than 0.07 mg/mL to use the minimal amount of protein needed to facilitate nanocrystal formation.[15,20,21,25]

EXPERIMENTAL SECTION

Reagents and Materials. Iron(III) chloride hexahydrate ($FeCl_3 \cdot 6H_2O$, 98%) and iron(II) chloride tetrahydrate ($FeCl_2 \cdot 4H_2O$, 99.99%) were purchased from Sigma-Aldrich, and potassium chloride (KCl, 99%) and Tris base (99.8%) were purchased from Fisher Scientific. All the chemicals were used as received without further treatment. $FeCl_3$ and $FeCl_2$ stock solutions were degassed and purged with nitrogen prior to use.

The mature form of Mms6 protein used in this study was expressed with a poly(histidine) tag (His-tag) on its N-terminal end.[20,21] His-tagged m2Mms6 was generated by shuffling the hydroxyl/carboxyl containing amino acid residues in the C-terminal domain of His-tagged Mms6, such that m2Mms6 shares the same hydropathy profile as Mms6.[21,27] For simplicity, the His-tagged Mms6 and m2Mms6 are simply referred to as Mms6 and m2Mms6 (both consisting of 99 amino acid residues, molecular weight (MW) ≈ 10 kDa, average molecular volume $v_{mol} \approx 1.3 \times 10^4$ Å^3).[32] Mms6 and m2Mms6 were purified in inclusion bodies, refolded as previously reported,[20,21,27] and dissolved in the buffer BC100 (20 mM Tris, 100 mM KCl, pH 7.5). Proteins in BC100 were flash-frozen with liquid nitrogen and kept frozen prior to use.

Sample Preparation for X-ray Measurements. Two independent batches of Mms6 and m2Mms6 proteins were used for the SAXS study. Pure Mms6 and m2Mms6 solutions at pH 7.5 with concentrations of 0.067−10 mg/mL were prepared by dilution from stock solutions with BC100 buffer solution, and it was found that concentrations ≳0.67 mg/mL ensure repeatability of X-ray measurements. 1.0 mg/mL Mms6 and m2Mms6 at pH 3 were also prepared by adding small amount of HCl to the original samples (pH 7.5), in which we observed that one batch of Mms6 looked cloudy upon lowering the pH, while the other batches of Mms6 and m2Mms6 were clear, suggesting a metastable state of some Mms6 proteins susceptible to abrupt drop in pH. Nevertheless, independent experiments including DNA sequencing (of gene coding for Mms6 proteins), SDS-PAGE of purified and refolded proteins, and FPLC gel filtration chromatograpy show the integrity of the protein, albeit at a different aggregation state.

All the mixtures of proteins and iron contained 83 mM $FeCl_3$, 42 mM $FeCl_2$, 6.7 mM Tris, and 33 mM KCl with pH 2.1−2.3. In a typical preparation of the sample with 0.33 mg/mL Mms6, a glass vial was put in a glovebox and charged with 100 μL of degassed water, 50 μL of 500 mM $FeCl_3$, 50 μL of 250 mM $FeCl_2$, and 100 μL of 1.0 mg/mL Mms6 in BC100 buffer as reported.[21] Iron-containing solutions were sealed and maintained under nitrogen at 4 °C for storage. The samples were brought up to room temperature for 2−4 h prior to the scattering measurements. Several sample conditions were tested including (a) samples stored at 4 °C for 2 months, (b) samples stored at 4 °C for 3 days, and (c) freshly prepared samples, which were made with the same stock solutions of proteins at room temperature without use of a glovebox 2−4 h before measurements. All protein/iron solutions prepared at different times (2 months, 3 days, or 2−4 h prior to scattering) were clear, except for the samples with high protein concentrations (≳2.0 mg/mL) that visibly showed minute precipitates. The measurements of several mixtures of buffer and iron solutions without proteins were used as background.

SAXS Setup. SAXS data presented in this study were collected using the synchrotron radiation at the beamline 12ID-B (X-ray energy E = 14.0 keV) at the Advanced Photon Source (APS), Argonne National Laboratory, and were repeatable for each sample conditions. A preselected set of sample conditions were also repeated at 12BM-B (APS) (X-ray energy E = 12.0 keV) to further ensure the repeatability and reproducibility of the collected data. At the 12ID-B, a two-dimensional (2D) detector Pilatus2m was used and the scattering vector magnitude Q, ($Q = 4\pi \sin(\theta)/\lambda$, 2θ being the scattering angle and λ being the X-ray wavelength), was calibrated with silver behenate scattering. The sample solutions were loaded into a flow cell (capillary tube, 1 mm in diameter) that was vertically mounted and normal to the incident X-ray beam. Furthermore, a commonly used, calibrating-protein standard, namely, lysozymes (prepared in NaOAc buffer, 40 mM NaOAc, 150 mM NaCl; pH 3.8), were used to validate the calibration of the SAXS apparatus. During the X-ray exposure period, the solutions flows at a constant rate controlled by a Hamilton Microlab 600 diluter. For each sample condition, multiple frames (30

DOI: 10.1021/la5044377
Langmuir 2015, 31, 2818−2825

frames) of scattering were collected to ensure data reproducibility and were later averaged to improve counting statistics. Exposure time (2 s) per frame was carefully chosen to minimize radiation damage while still providing acceptable signal/noise ratio. The 2D data were converted to one-dimensional (1D) plots of intensity versus Q. Most data were collected within Q range 0.005−0.5 Å^{-1}. A number of selected samples were even measured to an extended Q range up to 1 Å^{-1}. The recorded scattering intensity is further corrected for background subtraction and normalization (to incident beam intensity and exposure time).[30,33,34] In this study, the aqueous solutions of Tris/KCl with or without iron are considered as a uniform medium and protein and protein−iron compounds are embedded scattering particles of interest in the medium. All SAXS intensities for the protein and protein/iron particles shown below are obtained by subtraction of a corresponding signal from the bare solutions without the protein and referred to as $I(Q)$ hereafter.

RESULTS AND DISCUSSION

Mms6 and m2Mms6 Assemblies in the Absence of Iron. SAXS intensities of Mms6 proteins at three concentrations, i.e., 0.67, 1, and 2 mg/mL, are shown in Figure 1a. Within the measured Q-range, the SAXS intensities scale proportionally with the Mms6 concentrations. Figure 1b shows that the SAXS intensities for different Mms6 concentrations overlap after normalization to the concentrations except for the large Q range. This indicates that the particles formed by proteins (characterized with the aggregation number n_{agg}) suspended in the solutions are not correlated and can be viewed as free particles as expected in the dilute solution limit where the scattering intensity is proportional to the number concentration, that is

$$I(Q) \propto N \times n_{agg} \times (\Delta\rho \times v_{mol})^2 \times P(Q) \quad (1)$$

where N is the total number of protein molecules in the irradiated solution volume. $P(Q)$ is the form factor of a single, isolated particle, which depends only on particle size and shape, and $P(0) = 1$. $\Delta\rho$ is the excess scattering length density (SLD) of a particle with respect to that of the medium, i.e., solution. A semiquantitative examination of the SAXS intensities shows three prominent Q-regimes, in each of which the scattering is characteristic of a power-law, i.e., $I(Q) \propto Q^{-\alpha}$, where $\alpha = 0, 4, 2$, for $Q < Q_L$, $Q_L < Q < Q_M$, and $Q_M < Q < Q_H$, as indicated in Figure 1a. The power-law features for $Q < Q_M$ can be analyzed empirically by the Guinier-Porod (GP) model.[35,36] The GP model, an approximation of $P(Q)$, combines the Guinier-law feature of scattering intensity at low-Q regime which determines the global shape and size of the particle at relatively large length scale, and the Porod-law feature at the relatively high-Q regime which provides the more local structural information at smaller length scales.[30,33,34] The GP model provides an average radius of gyration R_g and the inherent polydispersity of the scattering particles that causes the smearing and disappearance of the oscillations at the Porod-law regime on scattering from monodisperse solid spheres with sharp surfaces.[35,36] At low-Q, the GP model is given by $P(Q) \propto Q^{-s} \exp(-Q^2R_g^2/3)$, while at higher-$Q$, the $P(Q) \propto Q^{-d}$. As a first step in the analysis, we fit the SAXS intensity with a curve using the GP model with R_g = 50 Å, $s = 0$, and $d = 4$, corresponding to a solid, spherical scattering particle ($s = 0$) (Figure 1) with sharp surface ($d = 4$), with some deviations at both low-Q and high-Q. The $s = 0$ at Guinier-law regime unequivocally suggests the protein particles are approximately spherical (generally, $s = 1$ and $s = 2$ behaviors correspond to rod- or disk-like particles). A better fit of the SAXS intensities in the low-Q, Guinier-law regime ($Q < Q_L$) results in a larger R_g value, but it underestimates the intensity at the high-Q (Porod-law regime, i.e., $Q_L < Q < Q_M$), and vice versa. This is a direct consequence of the reciprocity between the size of the scattering objects and the spread of scattering intensity in reciprocal Q-space. A rule of thumb states that the SAXS intensity is concentrated on $Q < 2\pi/L$ for a scattering object of average size L.[30] The fact that a single apparent R_g of GP model fails to fit the SAXS data in the entire selected Q-regime suggests a broader polydispersity than the one neglected in the GP-model. The Q^{-2}-dependence at $Q_M < Q < Q_H$ is reminiscent of the Debye function for scattering of a Gaussian polymer chain which gives rise to Q^{-2} dependence in the high-Q regime.[33,34] In view of these observations, we use the core−corona model developed by Pedersen originally for block copolymer micelles,[37] that in general can explain, at least qualitatively, all three regions of the SAXS mentioned above.

The core−corona model[37] assumes a micelle constructed of hydrophobic segments that are densely packed into a spherical core of radius R_{core} and N_{chain} slightly hydrophilic chains that are evenly distributed and attached to the surface of the spherical core and extend into the aqueous medium as an ideal polymer chain (referred to as a Gaussian chain) in θ-solvent with a characteristic radius of gyration R_{chain}, as depicted in Figure 2a. The scattering intensity from such a micelle, modeled as a

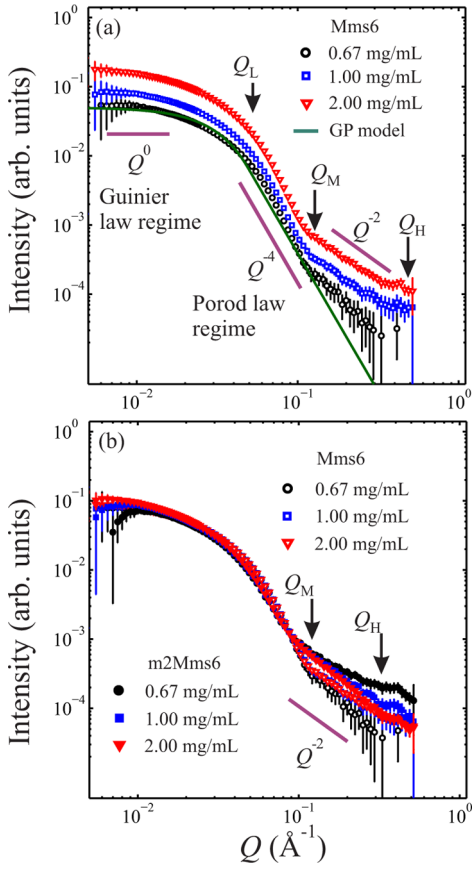

Figure 1. (a) SAXS intensities for Mms6 at 0.67, 1, and 2 mg/mL. (b) The SAXS intensities for Mms6 (empty symbols) and m2Mms6 (filled symbols) normalized to the concentrations. The symbols Q_L, Q_M, and Q_H indicate the boundaries of Q-ranges for different power-law behavior of scattering intensities. Three segments of slope 0, −2, and −4 are given as a guide to the eye.

DOI: 10.1021/la5044377
Langmuir 2015, 31, 2818−2825

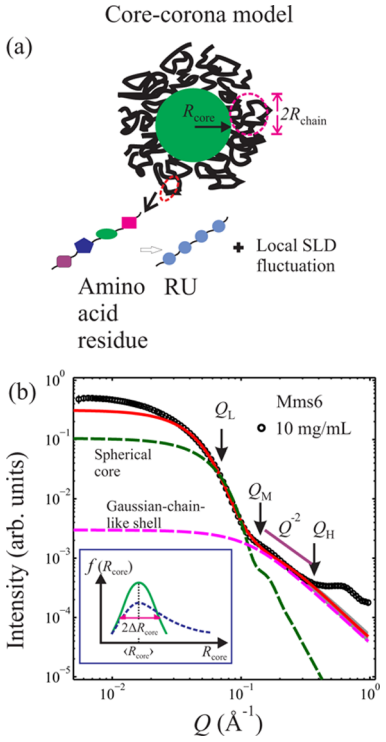

Figure 2. (a) Illustration of core−corona model. The spherical core is composed of densely packed, hydrophobic segments. The corona shell is approximated as Gaussian polymer chains attached on the core. Any deviations from the ideal Gaussian-polymer-chain model are viewed as only influencing locally structure on much smaller length scale. (b) SAXS intensity from a 10 mg/mL Mms6 solution. The solid (red) line is one of the best-model fitting curves in terms of eq 2. The narrow, gray area contains the model-fitting curves based on a range of structural parameters as follows: N_{chain} = 31 ± 14, $\langle R_{core}\rangle$ = 39 ± 4 Å, ΔR_{core} = 8 Å, R_{chain} = 11 ± 2 Å, and $\beta_{corona}/\beta_{core}$ = 0.9 ± 0.4. The SAXS intensity is mainly from scattering from the spherical core (green dashed line) at $Q_L < Q < Q_M$ and from the Gaussian chains in the corona (magenta dashed line) at $Q_M < Q < Q_H$. The segment of slope −2 serves as a guide to the eye. To account for particle polydispersity, a statistical distribution of R_{core} is assumed. The inset presents conceptual sketches of statistical distribution of R_{core}, $f(R_{core})$. The solid line in the inset is a sketch of a symmetrical, Gaussian-like distribution of R_{core} (centered at $\langle R\rangle$). The dashed line in the inset is a sketch of an asymmetric distribution in R_{core} that is skewed to large R_{core}. The additional portion in larger R_{core} with respect to the Gaussian distribution results in SAXS intensities concentrated more in small Q-regime while carrying negligible weights at high Q-regime.

function of Q, and paramtrized with R_{core}, R_{chain}, and so forth, is referred to as $I_1(Q; R_{core}, ...)$ and given by

$$I_1(Q; R_{core}, ...) \propto \beta_{core}^2 P_{core}(Q; R_{core}) + \frac{1}{N_{chain}}\beta_{corona}^2 P_{chain}(Q; R_{chain}) + \left(\frac{N_{chain}-1}{N_{chain}}\right)\beta_{corona}^2 S_{chain/chain}(Q; R_{core}, R_{chain}) + 2\beta_{corona}\beta_{core} S_{core/chain}(Q; R_{core}, R_{chain}) \quad (2)$$

where β_{core} and β_{corona} are the total number of excess scattering length in the core and corona, respectively. The core resembles a solid sphere and the corona chains resemble Gaussian polymer chains. Accordingly, the first two terms in eq 2, $P_{core}(Q, R_{core})$ and $P_{chain}(Q, R_{chain})$, correspond to the form factor of a solid sphere of radius R_{core} and a Gaussian chain of radius of gyration R_{chain}, respectively. The last two terms that contain $S_{chain/chain}(Q; ...)$ and $S_{core/chain}(Q; ...)$ represent contributions from chain−chain correlations in the corona and from chain−core correlation, respectively. Details of the functions can be found in ref 37. At $Q = 0$, $I_1(0) \propto (\beta_{core} + \beta_{corona})^2$, in which $(\beta_{core} + \beta_{corona})$ is the total excess scattering length of the micelle. As there are two types of scattering entities (core and corona chain) and there is no deterministic way of knowing the polydispersity of size in each, we only assume the core radius obeys a Gaussian distribution (see an illustration in Figure 2b), i.e., $f(R_{core}) = 1/((2\pi)^{1/2}\Delta R_{core}) \exp[-(R_{core} - \langle R_{core}\rangle)^2/2\Delta R_{core}^2]$, where $\langle R_{core}\rangle$ and ΔR_{core} represent the mean and spread of the core radius, respectively. So, the total scattering intensity from such a distribution of micelles, $I(Q)$, is proportional to $\int f(R_{core}) I_1(Q; R_{core}, ...)\, dR_{core}$.

By applying the core−corona model to protein particles, we assume that to a reasonable approximation structural variations among amino acids residues forming the corona can be neglected. Figure 2a depicts the protein as a sequence of amino acid residues, simplified to an idealized polymer chain of repeating units (RU) that are averaged over all amino acid residues. The deviation of SLD of the actual amino acid from that of the RU is restricted on a length scale of a few angstroms (dimension of an amino acid) and is expected to only influence the X-ray intensity at the wide angle regime. The N-terminal domain with multiple hydrophobic amino acid residues forms a core, and the C-terminal domain and His-tag, characterized with hydrophilic amino acid residues, form the corona, that give rise to the Q^{-2}-dependence of intensity at high-Q. Figure 2b shows that the solid line is the best fit using optimal parameters (N_{chain} = 31 ± 14, $\langle R_{core}\rangle$ = 39 ± 4 Å, ΔR_{core} = 8 Å, R_{chain} = 11 ± 2 Å, and $\beta_{corona}/\beta_{core}$ = 0.9 ± 0.4) based on eq 2, whereas the two dashed lines represent the contributions from the first term and second term in eq 2 to illustrate the principal contributions to the SAXS intensity at the two consecutive power-law regimes. At $Q_L < Q < Q_M$, the scattering is dominated by the core yielding the Q^{-4}-dependence, while at $Q_M < Q < Q_H$, the scattering is dominated by dangling residues that resemble Gaussian polymer chains with Q^{-2}-dependence. Given the radius of the core, the percentage of the protein chain contained in the core, and the average molecular volume of a single Mms6 (1.3×10^4 Å^3, calculated in terms of Mms6 amino acid sequence),[32] the aggregation number of the micelle (n_{agg}) is estimated to be 40 ± 10 at most based on the space-filling model, i.e., the core is constituted by densely packed protein segments. The apparent failure in fitting the SAXS data at $Q < Q_L$ suggests that the assumption of a symmetrical, Gaussian distribution in R_{core} underestimates the actual distribution that may contain substantially more particles with larger R_{core}. The deviation of the SAXS intensity at $Q > Q_H$, which appears for all samples, scales with concentrations originating from the details of the micelle structure at much smaller length scales. The peak at $Q \approx 0.65$ Å^{-1} corresponding to a repeat distance of ~10 Å is reproducible and likely related to a repeat unit in the protein of which the origin awaits further investigation.

Overlaying the SAXS patterns of Mms6 and m2Mms6 shows that the large-scale morphology of the two is similar, as demonstrated in Figure 1b. However, the high-Q regime shows that the differences between the two that, although subtle, may

DOI: 10.1021/la5044377
Langmuir 2015, 31, 2818−2825

be important to their affinity to iron, as has been observed in other studies.[21] After concentration normalization, the SAXS intensities at $Q < Q_M$ collapse into a single curve indicating that m2Mms6 and Mms6 have virtually similar micellar core. However, the $Q^{-\alpha}$-dependence over $Q_M < Q < Q_H$ (dictated by corona chains) for m2Mms6 is evidently different from that of wild-type Mms6, indicating that the corona chains of m2Mms6 deviate from an ideal Gaussian chain ($\alpha = 2$). Noting that a positive (negative) deviation from $\alpha = 2$ is indicative of unfavorable (favorable) chain−solvent interaction,[38] the observation of a positive deviation from $\alpha = 2$ for m2Mms6 at high concentration (2 mg/mL) suggests a more compact chain conformation, and the negative deviation for m2Mms6 at low concentration (0.67 mg/mL) suggests a more extended chain conformation. These subtle but important observations demonstrate that, while Mms6 and m2Mms6 form similar micellar cores, they arrange their amino acid residues in the C-terminal domains differently in the corona, namely, the functional region that primarily interacts with relevant ions to initiate crystal nucleation.

Protein−Iron Complexes (Particles) Produced by the Combination of Protein and Iron. The presence of iron in the protein solutions results in significant changes of the SAXS patterns compared to those of protein without iron in solution. Figure 3 shows SAXS from proteins in saturated iron solutions after the subtraction of the iron solution contribution thus representing the scattering from protein−iron complexes only. Figure 3a shows SAXS intensities of two independent preparations of Mms6 (labeled "prep-1", empty symbols using a single independent batch of Mms6, and "prep-2", filled symbols using a pooled preparation of four independent batches of Mms6). Within each preparation, the SAXS intensities overlay reasonably well upon normalization to concentration, indicating negligible correlations among protein−iron complexed particles. Whereas the SAXS of prep-1 shows some deviation from that of the pure protein (solid line) prep-2 shows a stronger deviation at the low-Q regime ($Q < Q_L$) with a power-law $Q^{-\alpha}$-dependence ($\alpha \approx 2$). We note that, in an independent study of a third preparation of Mms6/iron, the SAXS displayed the same $Q^{-\alpha}$-dependence ($\alpha \approx 2$) at the low-Q regime (data not shown) as in prep-2. The difference may be due to the presence of different levels of residual detergent molecules in the proteins.[39] A similar power-law feature at the low-Q regime is also observed for m2Mms6, as shown in Figure 3b. For the $Q_L < Q < Q_H$ region, the curves seem to almost coincide with those of the pure protein preparations, suggesting the original protein micelles remain almost intact in the presence of iron. At $Q_M < Q < Q_H$, the Q^{-2} dependence (except for the anomaly for prep-1) is characteristic of scattering from the polymer-coil-like structure.

The emergence of $Q^{-\alpha}$-dependence ($\alpha \approx 2$) intensities over the low-Q regime ($Q < Q_L$) can be interpreted as arising from the spatial correlation of the micelles. Two levels of structural hierarchy and complexities are presented as follows in a simplistic manner. In the absence of iron, as discussed in the preceding section, the total number N of proteins are dispersed in the irradiated volume to form N/n_{agg} micelles (first level of hierarchy), each of which scatters X-ray independently, as expressed in eq 1. In response to changes by the addition of iron ions, these free-roaming micelles interact with one another to form an assembly of a higher hierarchy. Assuming they remain intact after association, the intensity from these protein/iron particles, $I(Q)$, can be modeled as follows

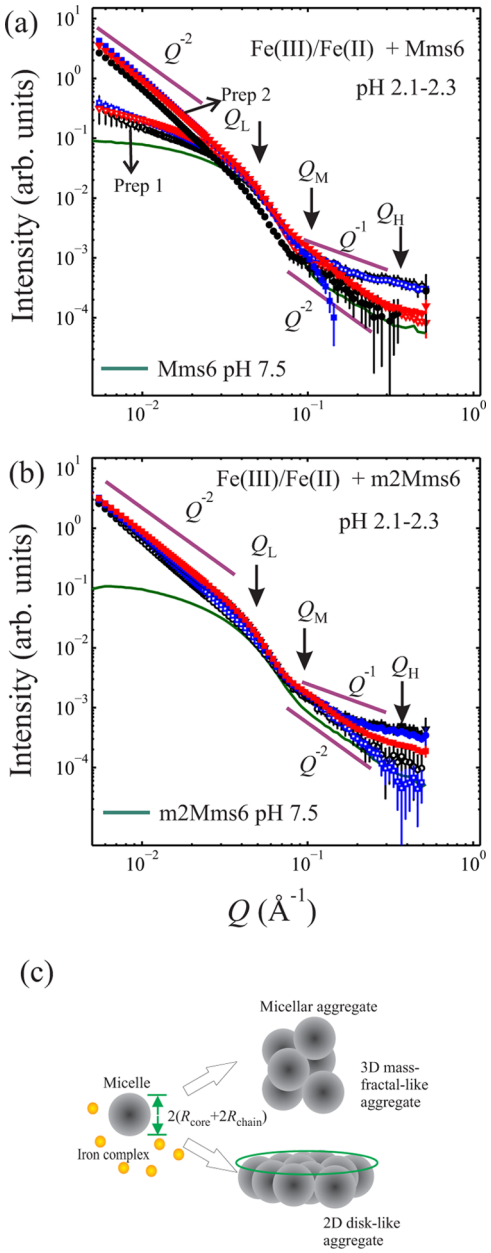

Figure 3. (a) Concentration-normalized SAXS data (iron background subtracted) for Mms6 solutions of 0.67 (◯), 1 (□), and 2 mg/mL (▽) in the presence of $FeCl_3$ and $FeCl_2$. The empty and filled symbols represent two preparations of Mms6, denoted prep 1 and 2, respectively. (b) Concentration-normalized SAXS data for m2Mms6 at 0.67 (◯), 1 (□), and 2 mg/mL (▽) in the presence of $FeCl_3$ and $FeCl_2$. The empty symbols and filled symbols represent solutions prepared 2 months and 3 days prior to SAXS measurements. The overlap of intensities suggests that the sample conditions in the presence of iron are stable. Solid lines represent scattering data collected at high pH (7.5) for comparison. The symbols Q_L, Q_M, and Q_H indicate the boundaries of Q-ranges for different power-law behavior of scattering intensities. (c) Illustration of aggregates made up of micelles as building blocks for $S(Q) \propto Q^{-2}$. Segments of slope −1 and −2 serve as a guide to the eye.

$$I(Q) \propto N \times n_{agg} \times (\Delta\rho \times v_{mol})^2 \times S(Q) \times P(Q) \quad (3)$$

where $S(Q)$ is referred to as structure factor accounting for the correlation among micelles.

DOI: 10.1021/la5044377
Langmuir 2015, 31, 2818−2825

The power-law in $I(Q)$ at $Q < Q_L$, i.e., $I(Q) \propto Q^{-\alpha}$ ($\alpha \approx 2$) is ascribed to $S(Q)$ for an assembly of building blocks (micelles, in this case) packed in an open, mass-fractal-like manner.[40] Mathematically, $S(Q)$ of a mass fractal dominates the intensity up to $Q \simeq a^{-1}$ below which $P(Q)$ is approximately unity, and a is a characteristic length of its building blocks.[40] For $Q \gtrsim a^{-1}$, $S(Q) \sim 1$ and eq 3 is reduced to eq 1.[40] This explains a new power-law for low-Q range ($Q < Q_L$) in Figure 3a,b. Alternatively, the $\alpha \approx 2$ at the low-Q regime is also consistent with lateral micelle association forming planar larger, disk-like objects. The total intensity for such a disk-like structure, in terms of the GP-model, is $Q^{-s} \exp(-Q^2R_g^2/3)$, where $s = 2$ for a disk-like object at low and medium Q range.[35,36] These two picures of the protein micellar assemblies are depicted as disk-like objects and mass-fractal-like aggregates in Figure 3c.

The fact that the scattering intensities at high-Q regime ($Q_M < Q < Q_H$) still exhibit a distinctive $Q^{-\alpha}$-dependence, albeit subtle deviations from $\alpha = 2$ and slightly higher than those for proteins in the absence of iron, indicates the existence of similar polymer-coil-like structure on a similar length scale of the corona chains on protein micelles. The corona giving rise to slightly higher intensities in the presence of iron may suggest SLD enhancement due to the iron enrichment, which necessitate validation by other techniques.

Introducing iron into a pH neutral aqueous solution results in significant pH reduction due to iron hydrolysis; therefore, we conducted control experiments under similar pH values in the absence of iron in solutions to evaluate the effect of pH alone on protein associations. Figure 4 shows a comparison of SAXS

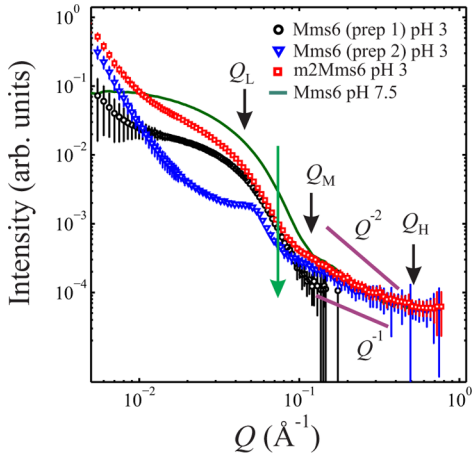

Figure 4. SAXS scattering from Mms6 and m2Mms6 at low pH (3) (only intensities that are substantially above background are shown). Solid lines represent scattering data collected at high pH (7.5) for comparison. The symbols Q_L, Q_M, and Q_H indicate the boundaries of Q-ranges for different power-law behavior of scattering intensities. The arrow (green) at $Q_L < Q < Q_M$ indicates the reduction in intensities supposedly from micelle cores upon lowering pH. Segments of slope −1 and −2 serve as a guide to the eye.

from Mms6 at various pH values (without iron in the solutions). The intensity profiles are clearly different than those shown in Figure 3 both in absolute intensity and in shape. Qualitative examination of the data at $Q_L < Q < Q_M$ suggests that lowering the pH has a dramatic effect on the protein structure. Although independent micelles may still be present in the solution, the lower intensity compared to that at pH 7.5 is evidence of a much lower core density of these micelles and deterioration of the core structure compared to micelles at pH 7.5. The observation of a weak peak in one of Mms6 preps at $Q \approx 0.05$ Å^{-1} may correspond to an average particle size of ∼120 Å in correlated aggregates, which is on the same length scale as that obtained from the core−corona model. Considering that the isoelectric point (IP) of Mms6 is ∼5.2, as calculated from its primary amino acid sequence, lowering the pH from 7.5 to 3.0 forces the protein to pass the IP abruptly. This may transform the micellar state to a metastable state that may lead to precipitation at low pH. At low-Q regime ($Q < Q_L$), the upturn in intensities is attributed to correlations between micelles, giving rise to a structure factor $S(Q)$, as in eq 3. At the high-Q regime that is supposedly dictated by the corona, the Q^{-2}-dependence of intensities is replaced by a Q^{-1}-dependence upon lowering the pH to 3, indicating a significant change in conformation of corona chains. The Q^{-1}-dependence is commonly regarded as originating from rod-like scattering objects.

CONCLUSIONS

Using synchrotron radiation SAXS, we determined the micellar morphology of the protein Mms6 that is implicated in promoting the growth of nanocrystal magnetite in magnetotactic bacteria. The morphology of Mms6 is compared with that of its mutant, m2Mms6, that does not bind iron, in Tris/KCl solutions with or without Fe(II) and Fe(III) in solutions. Our main results are summarized as follows: (1) The Mms6 and m2Mms6 proteins both aggregate as micelles that resemble core−corona structures of block polymer micelles. The core is likely formed by hydrophobic segments of the proteins and is modeled as a sphere of average radius ∼40 Å. The corona shell consists of hydrophilic residues that give rise to typical Gaussian-polymer-chain-like structure extending the radius of the core by ∼20 Å. We find subtle but relevant differences between the corona of Mms6 and its mutant m2Mms6, the charged regions of the protein responsible for the initial binding of ions and nucleation. (2) The presence of Fe(II)/Fe(III) ions in solutions to a large extent preserves the micellar structure in the absence of iron and induces weak association among micelles. This iron-induced association produces larger particles in the form of a disk-like particles or a mass-fractal-like structure. (3) While the morphology of the cores is similar, we qualitatively infer some differences in the corona conformation of the protein particles in the presence and absence of iron isolations. Relatively higher protein concentrations lead to aggregation, first into micelles at neutral pH, and into larger micellar aggregates in the presence of iron. (4) Control experiments at pH values that are comparable to those obtained by the addition of iron ions in solutions reduce core densities. By contrast, Fe ions in solutions at low pH values preserve the integrity of the micellar structure of the protein.

AUTHOR INFORMATION

Corresponding Authors

*E-mail: wwang@ameslab.gov.
*E-mail: suryakm@iastate.edu.

Notes

The authors declare no competing financial interest.

ACKNOWLEDGMENTS

We thank Xiaobin Zuo at beamline 12ID-B and Benjamin Reinhart at beamline 12BM-B of APS for technical support in

DOI: 10.1021/la5044377
Langmuir 2015, 31, 2818−2825

SAXS. We thank Pierre E. Palo (Ames Laboratory) for kindly preparing the proteins. Research supported by the U.S. Department of Energy, Office of Basic Energy Sciences, Division of Materials Sciences and Engineering. Ames Laboratory is operated for the U.S. Department of Energy by Iowa State University under Contract No. DE-AC02-07CH11358. Use of the Advanced Photon Source, an Office of Science User Facility operated for the U.S. Department of Energy (DOE) Office of Science by Argonne National Laboratory, was supported by the U.S. DOE under Contract No. DE-AC02-06CH11357.

REFERENCES

(1) Mann, S. *Biomineralization:Principles and Concepts in Bioinorganic Materials Chemistry*; Oxford University Press: New York, 2001.
(2) Veis, A. Crystals and Life: An Introduction. In *Biomineralization*; John Wiley & Sons, Ltd.: New York, 2010.
(3) Fratzl, P.; Weinkamer, R. Nature's Hierarchical Materials. *Prog. Mater. Sci.* **2007**, *52*, 1263−1334.
(4) Sarikaya, M.; Tamerler, C.; Jen, A. K. Y.; Schulten, K.; Baneyx, F. Molecular Biomimetics: Nanotechnology Through Biology. *Nat. Mater.* **2003**, *2*, 577−585.
(5) Cölfen, H.; Mann, S. Higher-Order Organization by Mesoscale Self-Assembly and Transformation of Hybrid Nanostructures. *Angew. Chem., Int. Ed.* **2003**, *42*, 2350−2365.
(6) Aizenberg, J.; Weaver, J. C.; Thanawala, M. S.; Sundar, V. C.; Morse, D. E.; Fratzl, P. Skeleton of *Euplectella* sp.: Structural Hierarchy from the Nanoscale to the Macroscale. *Science* **2005**, *309*, 275−278.
(7) Liu, X.; Mallapragada, S. K. Bioinspired Synthesis of Organic/Inorganic Nanocomposite Materials Mediated by Biomolecules. In *On Biomimetics*, Pramatarova, L., Ed.; InTech, 2011; pp229−250.
(8) Falini, G.; Albeck, S.; Weiner, S.; Addadi, L. Control of Aragonite or Calcite Polymorphism by Mollusk Shell Macromolecules. *Science* **1996**, *271*, 67−69.
(9) Belcher, A. M.; Wu, X. H.; Christensen, R. J.; Hansma, P. K.; Stucky, G. D.; Morse, D. E. Control of Crystal Phase Switching and Orientation by Soluble Mollusc-Shell Proteins. *Nature* **1996**, *381*, 56−58.
(10) Gordon, L. M.; Joester, D. Nanoscale Chemical Ttomography of Buried Organic-Inorganic Interfaces in the Chiton Tooth. *Nature* **2011**, *469*, 194−197.
(11) Bazylinski, D. A.; Frankel, R. B. Magnetosome Formation in Prokaryotes. *Nat. Rev. Micro.* **2004**, *2*, 217−230.
(12) Siponen, M. I.; Legrand, P.; Widdrat, M.; Jones, S. R.; Zhang, W.-J.; Chang, M. C. Y.; Faivre, D.; Arnoux, P.; Pignol, D. Structural Insight into Magnetochrome-Mediated Magnetite Biomineralization. *Nature* **2013**, *502*, 681−684.
(13) Fdez-Gubieda, M. L.; Muela, A.; Alonso, J.; García-Prieto, A.; Olivi, L.; Fernández-Pacheco, R.; Barandiarán, J. M. Magnetite Biomineralization in *Magnetospirillum gryphiswaldense*: Time-Resolved Magnetic and Structural Studies. *ACS Nano* **2013**, *7*, 3297−3305.
(14) Kolinko, I.; Lohsze, A.; Borg, S.; Raschdorf, O.; Jogler, C.; Tu, Q.; Posfai, M.; Tompa, E.; Plitzko, J. M.; Brachmann, A.; Wanner, G.; Muller, R.; Zhang, Y.; Schuler, D. Biosynthesis of Magnetic Nanostructures in a Foreign Organism by Transfer of Bacterial Magnetosome Gene Clusters. *Nat. Nanotechnol.* **2014**, *9*, 193−197.
(15) Arakaki, A.; Webb, J.; Matsunaga, T. A Novel Protein Tightly Bound to Bacterial Magnetic Particles in Magnetospirillum magneticum Strain AMB-1. *J. Biol. Chem.* **2003**, *278*, 8745−8750.
(16) Tanaka, M.; Mazuyama, E.; Arakaki, A.; Matsunaga, T. Mms6 Protein Regulates Crystal Morphology during Nano-sized Magnetite Biomineralization in Vivo. *J. Biol. Chem.* **2011**, *286*, 6386−6392.
(17) Wang, L.; Nilsen-Hamilton, M. Biomineralization Proteins: From Vertebrates To Bacteria. *Front. Biol.* **2013**, *8*, 234−246.
(18) Prozorov, T.; Bazylinski, D. A.; Mallapragada, S. K.; Prozorov, R. Novel magnetic nanomaterials inspired by magnetotactic bacteria: Topical review. *Mater. Sci. Eng., R* **2013**, *74*, 133−172.
(19) Kashyap, S.; Woehl, T. J.; Liu, X.; Mallapragada, S. K.; Prozorov, T. Nucleation of Iron Oxide Nanoparticles Mediated by Mms6 Protein in Situ. *ACS Nano* **2014**, *8*, 9097−9106.
(20) Prozorov, T.; Mallapragada, S. K.; Narasimhan, B.; Wang, L.; Palo, P.; Nilsen-Hamilton, M.; Williams, T. J.; Bazylinski, D. A.; Prozorov, R.; Canfield, P. C. Protein-Mediated Synthesis of Uniform Superparamagnetic Magnetite Nanocrystals. *Adv. Funct. Mater.* **2007**, *17*, 951−957.
(21) Wang, L.; Prozorov, T.; Palo, P. E.; Liu, X.; Vaknin, D.; Prozorov, R.; Mallapragada, S.; Nilsen-Hamilton, M. Self-Assembly and Biphasic Iron-Binding Characteristics of Mms6, A Bacterial Protein That Promotes the Formation of Superparamagnetic Magnetite Nanoparticles of Uniform Size and Shape. *Biomacromolecules* **2011**, *13*, 98−105.
(22) Prozorov, T.; Palo, P.; Wang, L.; Nilsen-Hamilton, M.; Jones, D.; Orr, D.; Mallapragada, S. K.; Narasimhan, B.; Canfield, P. C.; Prozorov, R. Cobalt Ferrite Nanocrystals: Out-performing Magnetotactic Bacteria. *ACS Nano* **2007**, *1*, 228−233.
(23) Amemiya, Y.; Arakaki, A.; Staniland, S. S.; Tanaka, T.; Matsunaga, T. Controlled Formation of Magnetite Crystal by Partial Oxidation of Ferrous Hydroxide in the Presence of Recombinant Magnetotactic Bacterial Protein Mms6. *Biomaterials* **2007**, *28*, 5381−5389.
(24) Arakaki, A.; Masuda, F.; Amemiya, Y.; Tanaka, T.; Matsunaga, T. Control of the Morphology and Size of Magnetite Particles with Peptides Mimicking the Mms6 Protein from Magnetotactic Bacteria. *J. Colloid Interface Sci.* **2010**, *343*, 65−70.
(25) Galloway, J. M.; Arakaki, A.; Masuda, F.; Tanaka, T.; Matsunaga, T.; Staniland, S. S. Magnetic Bacterial Protein Mms6 Controls Morphology, Crystallinity and Magnetism of Cobalt-Doped Magnetite Nanoparticles in Vitro. *J. Mater. Chem.* **2011**, *21*, 15244−15254.
(26) Galloway, J. M.; Bramble, J. P.; Rawlings, A. E.; Burnell, G.; Evans, S. D.; Staniland, S. S. Biotemplated Magnetic Nanoparticle Arrays. *Small* **2012**, *8*, 204−208.
(27) Feng, S.; Wang, L.; Palo, P.; Liu, X.; Mallapragada, S.; Nilsen-Hamilton, M. Integrated Self-Assembly of the Mms6 Magnetosome Protein to Form an Iron-Responsive Structure. *Int. J. Mol. Sci.* **2013**, *14*, 14594−14606.
(28) Wang, W.; Bu, W.; Wang, L.; Palo, P. E.; Mallapragada, S.; Nilsen-Hamilton, M.; Vaknin, D. Interfacial Properties and Iron Binding to Bacterial Proteins That Promote the Growth of Magnetite Nanocrystals: X-ray Reflectivity and Surface Spectroscopy Studies. *Langmuir* **2012**, *28*, 4274−4282.
(29) Rambo, R. P.; Tainer, J. A. Super-Resolution in Solution X-Ray Scattering and Its Applications to Structural Systems Biology. *Annu. Rev. Biophys* **2013**, *42*, 415−441.
(30) Svergun, D. I.; Koch, M. H. J.; Timmins, P. A.; May, R. P. *Small Angle X-ray and Neutron Scattering from Solutions of Biological Macromolecules*; Oxford Science Publications: Oxford, U.K., 2013; pp 13−26 and 65−88.
(31) Laurent, S.; Forge, D.; Port, M.; Roch, A.; Robic, C.; vander Elst, L.; Muller, R. N. Magnetic Iron Oxide Nanoparticles: Synthesis, Stabilization, Vectorization, Physicochemical Characterizations, and Biological Applications. *Chem. Rev.* **2008**, *108*, 2064−2110.
(32) Online peptide property calculator http://www.basic.northwestern.edu/biotools/proteincalc.html
(33) Narayanan, T. In *Soft Matter Characterization*; Borsali, R., Pecora, R., Eds.; Spring-Verlag: Berlin, 2008; pp 899−952.
(34) Als-Nielsen, J., McMorrow, D. *Elements of Modern X-ray Physics*; John Wiley & Sons: London, 2011.
(35) Hammouda, B. A New Guinier-Porod Model. *J. Appl. Crystallogr.* **2010**, *43*, 716−719.
(36) Hammouda, B. Analysis of the Beaucage Model. *J. Appl. Crystallogr.* **2010**, *43*, 1474−1478.
(37) Pedersen, J. S. Structure Factors Effects in Small-Angle Scattering from Block Copolymer Micelles and Star Polymers. *J. Chem. Phys.* **2001**, *114*, 2839−2846.
(38) Rubinstein, M.; Colby, R. H. *Polymer Physics*; Oxford University Press: Oxford, 2003.

DOI: 10.1021/la5044377
Langmuir 2015, 31, 2818−2825

(39) Note: In this study, Tergitol-type NP-40 detergent, as a solubilizing agent for membrane proteins, was used during the protein purification stage. In prep-1, special attention was given to lowering the potential residual levels of NP-40 to the lowest possible. Both prep-1 and prep-2 present same SAXS intensity profiles in the absence of iron.

(40) Teixeira, J. Small-Angle Scattering by Fractal Systems. *J. Appl. Crystallogr.* **1988**, *21*, 781−785.

DOI: 10.1021/la5044377
Langmuir 2015, 31, 2818−2825